



# Enhanced weathering of glacial rock flour drives coupled inorganic and organic carbon sequestration in a five-year field experiment

Christiana Dietzen<sup>1</sup>, Malgorzata Rizzi<sup>1</sup>, Tim Jesper Suhrhoff<sup>2,3</sup>, Minik Thorleif Rosing<sup>1</sup>

<sup>1</sup>Globe Institute, University of Copenhagen, 1350 Copenhagen, Denmark

5 <sup>2</sup> Yale Center for Natural Carbon Capture, Yale University, New Haven, CT, 06511, USA

<sup>3</sup> Department of Earth & Planetary Sciences, Yale University, New Haven, CT, 06511, USA

*Correspondence to:* Christiana Dietzen (christiana.dietzen@sund.ku.dk)

**Abstract.** Enhanced rock weathering (ERW) has been proposed as a scalable carbon dioxide removal strategy, yet long-term  
10 field-based constraints on weathering rates and associated carbon sequestration remain limited. Here, we present a five-year  
field assessment of Greenlandic glacial rock flour (GRF) applied at 50 t ha<sup>-1</sup> to a sandy agricultural soil in Denmark. Using a  
soil mass balance approach, we estimate that approximately 56% of the applied GRF dissolved over five years. Initial uptake  
of CO<sub>2</sub> via ERW is estimated at 3.2-4.9 t CO<sub>2</sub> ha<sup>-1</sup> when accounting for carbonate speciation in the acidic soil solution. If  
15 downstream transport of weathering products and subsequent re-equilibration with the more alkaline marine carbonate  
system is assumed, the estimated long-term atmospheric CO<sub>2</sub> removal increases to 6.39 t CO<sub>2</sub> ha<sup>-1</sup>. In addition to inorganic  
carbon removal, GRF-treated plots exhibited a significant increase in soil organic carbon stocks, equivalent to the storage of  
an additional 18.3 t CO<sub>2</sub> ha<sup>-1</sup>, with gains primarily associated with the mineral-associated organic matter fraction. These  
results demonstrate substantial weathering and carbon sequestration over five years under field conditions in a temperate  
20 climate and suggest that both inorganic and organic carbon dynamics contribute meaningfully to the overall climate impact  
of ERW of GRF. The findings provide rare multi-year field constraints on ERW performance and underscore the importance  
of robust measurements for quantifying carbon removal in agricultural systems, representing the first implementation of  
mass balance methods within the framework of a randomized block design.



## 1 Introduction

Enhanced rock weathering (ERW) has emerged as a promising carbon dioxide removal (CDR) strategy that removes atmospheric CO<sub>2</sub> by accelerating the natural weathering of silicate minerals while simultaneously delivering agronomic co-  
30 benefits (Beerling et al., 2018; Hartmann et al., 2013). By enhancing the dissolution of silicate minerals in soils, ERW releases base cations and generates alkalinity, promoting the formation of dissolved inorganic carbon that may ultimately be transported to the ocean and stored for thousands of years (Köhler et al., 2010; Renforth and Henderson, 2017). Robust  
35 monitoring, reporting, and verification (MRV) of CO<sub>2</sub> uptake associated with ERW is essential both for assessing the real-world climate impact of ERW at scale and for enabling carbon crediting, investment, and broader financial support for ERW deployment (Beerling et al., 2025; Bijma et al., 2026; Clarkson et al., 2024). However, current uncertainties in the  
quantification of weathering rates directly translate into uncertainty in reported CDR, limiting the credibility and scalability of ERW as a climate mitigation strategy on the voluntary carbon market (VCM) and underscoring the need for reliable field-based methods to measure weathering.

40 Despite growing interest in ERW, long-term field-based estimates of weathering rates of applied silicate minerals under realistic agricultural conditions remain limited (Buma et al., 2026). Many current estimates of the rate and efficiency of ERW are derived from laboratory experiments, short-term mesocosm studies, or reactive transport modeling. While these approaches provide important mechanistic insight, they cannot fully capture the hydrological variability, plant-soil interactions, and seasonal leaching dynamics that govern weathering in the field. Although field trials are increasingly being  
45 established, multi-year datasets remain scarce (Beerling et al., 2024; Dupla et al., 2025; Larkin et al., 2022), and direct quantification of weathering over time horizons exceeding three to four years within statistically robust, replicated field experiments remains largely absent. Because weathering rates are expected to decrease as reactive surface area is depleted (Brantley, 2025; Calabrese et al., 2021; Power et al., 2025), longer-term field assessments are critical for constraining realistic weathering rates and associated carbon sequestration.

50 Among the materials investigated for ERW, Greenlandic glacial rock flour has gained attention due to its extremely fine particle size, high specific surface area, and compositional homogeneity. Because it is naturally fine-grained, it can be deployed without the energy-intensive grinding typically required for conventional ERW feedstocks. Glacial rock flour (GRF) has been shown to be an effective alternative to traditional ERW materials for both carbon capture and crop yield  
55 improvement (Dietzen and Rosing, 2023; Gunnarsen et al., 2023; Obour et al., 2024; Oppong Danso et al., 2025; Tingey et al., 2025). In previous work, we estimated that 7.9% of GRF applied to an organic farm in Denmark weathered over approximately three years (Dietzen and Rosing, 2023). That estimate was derived from repeated measurements of soil exchangeable Mg, which tracked the accumulation of weathering-derived Mg on the soil exchange complex and its subsequent decline following leaching, allowing cumulative mineral dissolution to be inferred over time using routine



60 agronomic soil analyses. However, because the approach relied on discrete soil measurements rather than direct  
measurements of leaching fluxes, some weathering-derived cations were likely exported from the soil before sampling  
events rather than being captured in the exchangeable pool, leading to an underestimation of cations released. This limitation  
is likely to be particularly relevant in sandy soils, where rapid drainage during rainfall events can promote substantial losses  
of weathering products from the soil exchange complex (Huang and Hartemink, 2020).

65  
To address these limitations, we reevaluated the weathering of GRF five years after its application using soil mass balance  
("SOMBA") methods developed since our initial analysis (Suhrhooff et al., 2025). These approaches, sometimes referred to as  
the "TiCAT" method (Reershemius et al., 2023; Suhrhooff et al., 2024), use immobile tracers such as Ti to quantify the  
contribution of applied material to the sampled soil volume. By comparing the inferred soil cation concentrations before  
70 weathering to observed concentrations at the time of sampling, SOMBA provides a means of distinguishing time-integrated  
loss of feedstock attributable to weathering from other losses. To date, these methods have not yet been applied within  
randomized block designs typical of agricultural field experiments, which can help mitigate within-site soil heterogeneity  
that may otherwise limit the reliability of SOMBA-based estimates of weathering. In this study, we present a framework for  
integrating SOMBA methods into randomized block field experiments to enable more robust estimation of weathering in  
75 ERW trials.

In addition to uncertainties in inorganic carbon generation, the overall carbon balance of ERW systems remains incompletely  
understood because potential effects on soil organic carbon (SOC) are rarely integrated into CDR assessments (Bijma et al.,  
2026; Vicca et al., 2022). ERW may influence SOC dynamics through multiple interacting pathways. Though research on  
80 changes in organic carbon fluxes in the context of ERW is limited, insights from liming studies (Wang et al., 2021; Zhang et  
al., 2022) may provide a useful analogue for understanding SOC responses to ERW, as both processes modify soil acidity  
and increase base cation availability. Liming experiments frequently report an initial pulse of SOC mineralization following  
increases in soil pH, but longer-term responses can include enhanced plant productivity, as observed in the first year of this  
experiment (Gunnarsen et al., 2023), greater belowground carbon inputs, and increased stabilization of microbial residues in  
85 mineral-associated organic matter (MAOM) (Paradelo et al., 2015). Consistent with this balance between enhanced carbon  
inputs and stimulated microbial turnover, experimental studies of silicate amendments have thus far reported both increases  
and decreases in SOC (Xu et al., 2025), highlighting the strong dependence of SOC responses on site conditions,  
mineralogy, and timescale and emphasizing the need for multi-year field observations. Among the potential mechanisms  
influencing SOC dynamics under ERW, organo-mineral interactions may be particularly important where the application of  
90 finely ground silicate materials substantially increases the availability of reactive mineral surface area.

Compared to other silicate feedstocks, the exceptionally high specific surface area of GRF ( $19.6 \text{ m}^2 \text{ g}^{-1}$ ) (Sarkar, 2021)  
introduces a substantial input of reactive mineral surfaces that could influence SOC stabilization through organo-mineral



interactions. Microbial processing of plant-derived inputs produces organic compounds that can bind to reactive mineral  
95 surfaces through sorption and organo-mineral interactions, forming MAOM that is less prone to rapid decomposition  
(Basile-Doelsch et al., 2020; Kleber et al., 2021). Such processes may be particularly relevant in coarse-textured sandy soils,  
which typically contain low clay fractions, limited abundance of reactive secondary minerals, and correspondingly low  
specific surface area, constraining MAOM formation by limiting the availability of mineral surfaces capable of stabilizing  
organic compounds (Georgiou et al., 2025; Six et al., 2002). In such systems, the addition of finely ground silicate material  
100 could disproportionately increase mineral surface area relative to the native soil matrix and potentially enhance opportunities  
for organo-mineral stabilization.

Despite these hypothesized mechanisms, the net effect of ERW on SOC remains poorly constrained under field conditions,  
particularly over multi-year timescales. Resolving these dynamics requires long-term experiments that simultaneously  
105 quantify both inorganic carbon removal through weathering and potential changes in soil organic carbon pools. Here, we  
reassess the weathering of GRF five years after application at the Vojens field site using the SOMBA soil mass balance  
framework, representing the first application of SOMBA within a replicated, randomized block design field experiment.  
Using this approach, we determine the dissolution fraction of GRF after five years, revise estimates of associated inorganic  
CO<sub>2</sub> sequestration, and assess changes in total and fractionated SOC to evaluate potential organic carbon responses to GRF  
110 application. By integrating long-term field measurements of both inorganic and organic carbon pools, this study provides a  
comprehensive assessment of the carbon sequestration potential of GRF under temperate agricultural conditions.

## 2. Materials and Methods

### 2.1 Study Site and Experimental Design

The study was established in 2019 on an organic farm in Vojens, Denmark (55.204556, 9.265528) (Dietzen and Rosing,  
115 2023; Gunnarsen et al., 2023). The soils at the site are classified as Cambic Arenosols with a loamy sand texture, formed  
from glacial outwash sands (Surface Geology Map of Denmark 1:25.000, 2022). These soils have a relatively low cation  
exchange capacity of 7.16 cmol<sub>c</sub> kg<sup>-1</sup> and high base saturation (~90%) (Dietzen et al., 2022). The mean annual temperature  
during the years in which the experiment took place (2019-2024) was 9.4° C and the mean annual precipitation was 968 mm  
yr<sup>-1</sup> (Vejrarkiv, 2026). Treatments included GRF applied at 10 and 50 t ha<sup>-1</sup> along with a control arranged as a randomized  
120 block design with four replicates, but only the 50 t ha<sup>-1</sup> treatments were analyzed using the SOMBA method in this study.  
The 10 t ha<sup>-1</sup> treatment was excluded from this re-analysis due to the limited sensitivity of the SOMBA method at lower  
application rates (Suhrhoff et al., 2024). GRF treatments were applied by hand to 1 m<sup>2</sup> quadrants to ensure uniform  
application rates across the 3 x 20 m plots. Full details of the experimental setup, including additional treatments not relevant  
to this analysis, can be found in Gunnarsen et al. (2023).



## 125 2.2 Glacial rock flour

The glacial rock flour (GRF) used in this experiment was sourced from the Ilulialik locality in Greenland (64.782806, -50.625806). The material has an extremely fine grain size ( $d_{50} = 2.6 \mu\text{m}$ ) and a high specific surface area (BET SSA =  $19.6 \text{ m}^2 \text{ g}^{-1}$ ) (Sarkar, 2021). Mineralogically, the material is primarily derived from felsic bedrock and consists of approximately 27.4% biotite, 18.6% oligoclase/andesine, 14.6% amphibole, 14.1% anorthite, 10.5% quartz, 4.3% Fe-oxide, 2.8% K-feldspar, and 2.4% muscovite, as determined by scanning electron microscopy (ZEISS Sigma 300VP Field Emission SEM; Geological Survey of Denmark and Greenland). Further information regarding the material can be found in Dietzen & Rosing (2023) and Sarkar (2021).

## 2.3 Soil Sampling and Analysis

135 Soil samples were collected on March 20<sup>th</sup>, 2024, approximately five years after the GRF was originally applied on April 17<sup>th</sup>, 2019. The soil had recently been ploughed before sampling, on March 12<sup>th</sup>. According to the farmer, the field was typically ploughed to a depth of 22-25 cm. Soil cores of a known volume were collected to a depth of 30 cm using an AMS Gator Core (American Falls, ID, USA), with five cores taken randomly along the length of each plot composited to form one representative sample per plot. Soil samples were dried at 40°C and weighed to determine bulk density based on the known volume of the soil core. After sieving to 2 mm, subsamples were taken for chemical analyses. Soil  $\text{pH}_{\text{H}_2\text{O}}$  was measured in a 1:2.5 soil-to-water ratio.

## 2.4 Bulk Elemental Analysis

Bulk elemental composition of the GRF and soil (Dietzen et al., 2026) was determined by ICP-OES following lithium metaborate fusion (Carignan et al., 2001) at the Centre de Recherches Pétrographiques et Géochimiques (CRPG), CNRS, Nancy, France. These elemental data were used to estimate dissolution fractions within the SOMBA framework (Reershemius et al., 2023; Suhrhoff et al., 2025). Exchangeable cations were not extracted in advance of analysis.

Loss on ignition (LOI) of soil and GRF was determined on separate subsamples by heating the material to 1000 °C for 5 hours in order to quantify mass loss due to the combustion of organic matter and the release of remaining bound water and other volatile components that were not removed during prior drying. Elemental concentrations were subsequently normalized to a volatile-free basis prior to use in mass balance calculations by correcting for LOI, such that concentrations represent the composition of the residual mineral fraction only. This correction ensures that comparisons between treated and control soils are not biased by differences in moisture content or organic matter, which would otherwise dilute elemental concentrations on a bulk mass basis. Bulk density values used in the SOMBA framework were likewise adjusted to a volatile-free basis to ensure consistency between mass-based elemental concentrations and soil mass calculations. Inferred



application rates were subsequently converted back to an initial mass basis including volatile components to correspond to the material as weighed and applied in the field.

The corrected elemental composition and maximum theoretical CO<sub>2</sub> uptake (CO<sub>2Max</sub>) of GRF are presented in Table 1.

160 CO<sub>2Max</sub> represents the maximum theoretical CO<sub>2</sub> sequestration potential (kg CO<sub>2</sub> t<sup>-1</sup> rock) assuming stoichiometric conversion of carbonic acid to bicarbonate for all released base cations (Mg<sup>2+</sup>, Ca<sup>2+</sup>, K<sup>+</sup>, and Na<sup>+</sup>). Unlike most ERW studies, CO<sub>2Max</sub> values were not adjusted using an ocean equilibration correction factor (Renforth and Henderson, 2017). Instead, carbonate speciation effects were accounted for explicitly during inorganic CO<sub>2</sub> uptake calculations, as described below.

165 Because the GRF contains a minor NaCl component, sodium concentrations were corrected to exclude the fraction associated with NaCl prior to calculation of CO<sub>2Max</sub> uptake and dissolution fractions. Chlorine concentrations were used to estimate Na present as NaCl, assuming all Cl occurs as NaCl, and this Na fraction was subtracted from total Na. Only silicate-bound Na was included in subsequent SOMBA mass balance calculations.

170 **Table 1. Average composition of glacial rock flour from the Ilulialik locality in Greenland. Reported concentrations are mean ± standard deviation (n = 9), normalized to 100% after correction for loss on ignition. Na<sub>2</sub>O values were corrected to exclude the fraction of Na associated with the minor NaCl component of the material. CO<sub>2Max</sub> represents the maximum theoretical CO<sub>2</sub> sequestration potential (kg CO<sub>2</sub> per t rock) assuming stoichiometric conversion of carbonic acid to bicarbonate for all released base cations (Mg<sup>2+</sup>, Ca<sup>2+</sup>, K<sup>+</sup>, and Na<sup>+</sup>). Non-corrected values are available in Dietzen et al. (2026).**

SiO <sub>2</sub>	Al <sub>2</sub> O <sub>3</sub>	Fe <sub>2</sub> O <sub>3</sub>	MnO	MgO	CaO	Na <sub>2</sub> O	K <sub>2</sub> O	P <sub>2</sub> O <sub>5</sub>	TiO <sub>2</sub>	CO <sub>2Max</sub> kg t <sup>-1</sup>
56.1%	16.8%	8.81%	0.12%	5.07%	3.85%	3.38%	3.56%	0.75%	0.13%	252
± 0.3	± 0.1	± 0.06	± 0.001	± 0.05	± 0.03	± 0.02	± 0.04	± .01	± 0.004	± 1.6

175

## 2.5 Soil Carbon Fractionation and Analysis

Particulate organic matter (POM) and mineral-associated organic matter (MAOM) fractions were separated based on particle size using a wet-sieving procedure following chemical dispersion, adapted from established protocols (Cambardella and Elliott, 1992; Lopez-Sangil and Rovira, 2013; Sanderman et al., 2013; Yu, 2022). Briefly, 10 g of dry, homogenized soil was dispersed in 50 ml of 0.5% sodium hexametaphosphate and mixed on a vertical rotating mixer for 18 h to disrupt macro- and microaggregates. Immediately prior to wet sieving, samples were sonicated for 15 min and then wet-sieved over a 53 µm mesh using Milli-Q water to separate the coarse POM fraction (>53 µm) from the fine MAOM fraction (<53 µm).



185 To ensure complete dispersion and separation of mineral material, particularly GRF associated with coarse organic matter, the retained POM fraction was re-dispersed in 10 ml of 0.5% sodium hexametaphosphate, sonicated for 5 min, mixed for an additional 30 min, and sonicated again for 10 min prior to a second wet-sieving step over a 53  $\mu\text{m}$  mesh. Material passing through the sieve during this re-fractionation was combined with the MAOM fraction from the initial separation, while material remaining on the sieve was classified as POM. Final fractions were dried at 60  $^{\circ}\text{C}$  and weighed for mass balance calculations. The MAOM mass was corrected for the sodium hexametaphosphate added during dispersion.

190

Organic carbon concentrations were determined for both bulk soil samples and the separated POM and MAOM fractions. Bulk soil subsamples were ball-milled prior to analysis, whereas POM and MAOM samples were ground manually in an agate mortar. 250 mg of each sample was decarbonized with 10% HCl to remove inorganic carbon, after which they were dried at 105  $^{\circ}\text{C}$  for 3 h to remove residual acid. Carbon concentrations were measured in triplicate using a Multi N/C 3100 - HT 1300 TOC/TNb analyzer (Analytik Jena, Germany), with combustion at 1300  $^{\circ}\text{C}$  under an  $\text{O}_2$  carrier gas flow of 2.2 L  $\text{min}^{-1}$  and detection by non-dispersive infrared (NDIR) spectroscopy. Based on repeated measurements of a certified reference material (NCS ZC71016; 22.3  $\text{g kg}^{-1}$ ;  $n = 6$ ), the relative standard deviation was 6.9%. Soil organic carbon (SOC) stocks ( $\text{t C ha}^{-1}$ ) were calculated on a fixed-depth basis (0-30 cm) using plot-specific bulk density measurements and the mean of triplicate SOC concentrations.

## 200 **2.6 Statistical analysis**

Categorical differences in measured parameters were assessed using linear mixed-effects models implemented in the ‘nlme’ package (Pinheiro et al., 2017) in R (R Core Team, 2023), all of which included block as a random effect. These models provided both formal hypothesis tests and the statistical inputs required for SOMBA-based calculations. Fixed effects were specified according to the comparison of interest, either distinguishing treated and control plots at the time of sampling or comparing observed treated concentrations with concentrations expected at the time of application, assuming no weathering. Residual plots were inspected to ensure the assumption of normality of residuals was met. Model-based summaries were obtained using estimated marginal means implemented in the ‘emmeans’ package in R (Lenth, 2022).

## 210 **2.7 Assessment of Signal Resolvability**

To assess signal resolvability, two distinct classes of linear mixed-effects models were fitted. First, treated-control contrasts were used to evaluate whether the increase in  $\text{Ti}$  due to feedstock application was statistically detectable despite background variability, which can be a challenge for SOMBA frameworks (Rogers and Maher, 2026). Demonstrating a resolvable immobile tracer signal is a prerequisite for application of the SOMBA framework, because this is used to infer the amount of applied material present in the sampled soil volume.



215 Because progressive dissolution causes concentrations of mobile cations in treated plots to converge toward control  
concentrations over time (Reershemius et al., 2023; Suhrhoff et al., 2025), treated-control contrasts of mobile elements are  
not appropriate for assessing weathering progression. Instead, for each cation, we used the SOMBA framework to  
reconstruct a block-specific baseline value for comparison with the observed concentrations in the treated plots. These values  
represented the expected cation concentrations if the amount of GRF inferred from the observed Ti increase were added to  
220 the corresponding control plot, without any loss due to weathering. A statistically significant deficit relative to this  
reconstructed baseline, as assessed via linear mixed-effects models, was interpreted as evidence of detectable cation loss due  
to weathering. Cations that did not exhibit such a deficit were not considered to provide a reliable constraint on weathering.

Mixed-effects models comparing treated and control plots were also fitted for each cation. Although not interpreted directly  
225 in terms of weathering, these models, along with the Ti model, provided treatment- and control-level means, variance  
components, block-level random effects, and residual distributions used as inputs for the SOMBA calculations and  
uncertainty propagation. As a result, the cation fraction that has not been lost ( $1-\tau$ ) includes cations that were released but are  
stored in secondary phases or on exchangeable sites, i.e., it may not represent un-dissolved feedstock exclusively.

## 2.8 Calculation of Dissolution Fractions

230 The fraction of GRF which was dissolved ( $\tau$ ) was quantified using a modified version of the SOMBA framework described  
by Suhrhoff et al. (2025), in which weathering is estimated by first inferring the contribution of applied feedstock to the soil  
from the concentration of an immobile tracer, such as Ti, measured in baseline soil, feedstock material, and treated post-  
weathering soils (Reershemius and Suhrhoff, 2023). As such, this approach also allows to infer the post-deployment but pre-  
weathering composition of the GRF and soil mix for treatment sites. We modified this approach by using concentrations  
235 measured in control and treated plots sampled contemporaneously as opposed to relying on paired before-and-after  
measurements from the same location. This change accounts for background processes that affected the entire field during  
the experimental period, such as the application of manure fertilizers to the entire field or seasonal biogeochemical cycling.  
Consequently, differences between control and treated plots can be directly attributed to the application and weathering of  
GRF, avoiding confounding effects that may arise when comparing samples collected several years apart from the same plot.

240

The increase in soil Ti concentrations was used to infer the amount of feedstock applied to the soil, which was subsequently  
used to reconstruct the expected concentration of mobile base cations in the soil before weathering. In this reconstruction, the  
cation concentrations measured in contemporaneously sampled control plots provide an estimate of the background soil  
composition at the time of sampling, which is assumed to represent the baseline composition in the absence of feedstock  
245 addition. The contribution of feedstock-derived cations inferred from the immobile tracer signal is then added to this baseline  
to estimate pre-weathering cation concentrations in treated plots for each block individually. Deviations between these



reconstructed pre-weathering concentrations and the observed cation concentrations at the time of sampling are attributed to weathering losses, enabling estimation of the dissolution fraction.

250 Furthermore, in contrast to previously published applications of SOMBA (Reershemius et al., 2023), we did not leach cations off the exchangeable sites but instead analyzed bulk soil samples. Hence, cations that were released during GRF weathering but are still stored on exchangeable sites or in secondary phases are still present in the samples. This has the benefit that  $\tau$  is a direct measure of realized CDR, reflecting cations that have been both released from the feedstock and transported out of the plough layer, without the need to account for CDR losses due to exchangeable processes or secondary  
255 phase formation within the system boundary.

The dissolution fraction ( $\tau$ ) and corresponding GRF application rate were calculated for each cation individually by inserting mean control and treated concentrations together with the site-average soil bulk density (also used to represent feedstock bulk density) into the SOMBA equations.

## 260 **2.9 Uncertainty Propagation**

Reported uncertainty was quantified using a parametric hierarchical bootstrap tailored to the randomized block design (Dietzen et al., 2026). Given the small number of blocks ( $n = 4$ ), model-based resampling was used to obtain stable variance estimates. This approach will likely always be necessary in similar experimental field trials, as the number of replicate blocks is unlikely to be high enough for non-parametric bootstrapping. Previously described linear mixed-effects models  
265 fitted to Ti and each mobile cation provided estimates of fixed effects, block-level random effects, and residual variability. For each of 3,000 bootstrap replicates, block-level random effects and residuals were resampled from the fitted mixed models and combined with the estimated fixed effects to generate synthetic control and treated observations. Within each bootstrap iteration, reconstructed concentrations were averaged across resampled blocks to obtain mean inputs for the SOMBA calculations. Bulk density was propagated analogously by resampling block-level bulk densities (mean of all plots  
270 within a block), with feedstock bulk density assumed equal to this value. Analytical uncertainty in feedstock composition was incorporated by sampling tracer concentrations from normal distributions defined by measured means and standard deviations (Table 1). The SOMBA equations were applied to each replicate to generate distributions of  $\tau$  and application rate, which were summarized using the standard deviation and 95% confidence intervals.

## **2.10 Determining inorganic CO<sub>2</sub> uptake**

275 In ERW studies, inorganic CO<sub>2</sub> uptake is commonly estimated either from bicarbonate generation and export from the soil system or from exported charge-balance alkalinity converted to long-term atmospheric CO<sub>2</sub> removal using established equilibration factors based on ocean carbonate speciation. As alkalinity is transported through soils, groundwater, and river systems toward the ocean, carbonate equilibria continuously adjust in response to changing pH and pCO<sub>2</sub> conditions



280 (Bertagni and Porporato, 2022; Zhang et al., 2025). Because the ocean is substantially more alkaline than the soil solution of most agricultural soils used for ERW, owing to both inherent soil acidity and elevated soil  $p\text{CO}_2$  (Dietzen and Rosing, 2023), the effective carbon-capture efficiency is likely to increase during downstream transport. This efficiency ultimately approaches the ocean-buffered conversion factor used in most ERW studies, which typically apply ocean correction factors of ranging from 80-90% (Bertagni and Porporato, 2022; Kanzaki et al., 2023; Renforth and Henderson, 2017). However, when carbonate speciation under soil conditions is also accounted for explicitly, sequential application of both soil- and  
285 ocean-based correction factors may inadvertently over-correct carbon-capture efficiency, as these corrections are not additive. Here, initial inorganic  $\text{CO}_2$  uptake is quantified at the point of alkalinity generation in the soil solution where GRF dissolution occurs, while longer-term atmospheric removal after downstream transport and equilibration with ocean carbonate chemistry is considered separately.

290 In Dietzen & Rosing (2023), we introduced a framework to estimate the fraction of mineral-derived base cations balanced by bicarbonate generation under soil conditions. Mineral dissolution in soils is driven by multiple proton sources, including carbonic acid as well as other inorganic and organic acids (Holden et al., 2024). These acids contribute to the total proton supply for weathering and influence carbonate speciation in the soil solution. Consequently, only a fraction of mineral-derived base cations is balanced by bicarbonate formation, meaning that the carbon-capture efficiency of weathering depends  
295 on the chemical conditions of the soil solution. The correction framework is based on carbonate system equilibria and uses soil pH and  $p\text{CO}_2$  to estimate the fraction of mineral dissolution that generates bicarbonate, conceptually similar to the alkalization carbon-capture efficiency (ACE) factor defined by Bertagni and Porporato (2022).

In Dietzen & Rosing (2023), laboratory-measured soil pH values were used directly. However, these measurements are  
300 determined under equilibrium with atmospheric  $p\text{CO}_2$  (~400 ppm) and therefore do not represent *in situ* soil conditions, where  $p\text{CO}_2$  is typically elevated (Elberling and Matthiesen, 2007; Matthiesen, 2004). Because carbonate speciation depends on both pH and  $p\text{CO}_2$ , failure to account for elevated soil  $p\text{CO}_2$  can bias estimates of bicarbonate generation efficiency. This bias causes the fraction of dissolution that generates bicarbonate to be overestimated when laboratory-measured soil pH ( $\text{pH}_{\text{H}_2\text{O}}$ ) exceeds approximately 5.6 and underestimated when it falls below this value.

305 In the updated framework,  $\text{pH}_{\text{H}_2\text{O}}$  values are first recalculated to reflect equilibrium with *in situ* soil  $p\text{CO}_2$  (see Dietzen et al., 2026 for calculator). These adjusted pH values are then used, together with the corresponding  $p\text{CO}_2$ , to estimate the fraction of mineral dissolution that generates carbonate alkalinity based on carbonate system equilibria in the soil solution. When selecting the input  $\text{pH}_{\text{H}_2\text{O}}$  values, it is important to account for both differences between treated and control soils and  
310 temporal variation in soil pH. To address this variability, we employed a site-specific range of  $\text{pH}_{\text{H}_2\text{O}}$  values in combination with a broad range of  $p\text{CO}_2$  values (1,000–40,000 ppm) to define upper and lower bounds for the correction factor at this site. Because direct measurements of soil  $p\text{CO}_2$  were not available and soil  $p\text{CO}_2$  varies spatially and temporally, this range-



based approach was used to bound uncertainty in the correction factor. The resulting predicted *in situ* pH values were then used, together with the corresponding input soil pCO<sub>2</sub> values, to calculate a range of bicarbonate generation efficiencies.

315

The bicarbonate generation estimated through this framework using soil pH and pCO<sub>2</sub> as inputs represents the initial CO<sub>2</sub> uptake associated with ERW under the carbonate chemistry conditions of the soil solution prior to transport of weathering products. However, on longer-term timescales the atmospheric impact will depend on the net charge-balance alkalinity exported from the terrestrial system and the carbonate speciation conditions under which that alkalinity ultimately equilibrates, primarily in the ocean (Kanzaki et al., 2023; Renforth and Henderson, 2017). The timescale over which this equilibration occurs is both uncertain and highly variable across systems, such that the appropriate correction factor and associated crediting timescale must be evaluated on a case-by-case basis.

320

Accordingly, we report inorganic CO<sub>2</sub> uptake as a range bounded by (i) the initial bicarbonate generation estimated from carbonate equilibria under soil solution conditions and (ii) long-term atmospheric removal after equilibration with ocean carbonate chemistry. These estimates do not deduct cations temporarily taken up by plants, under the simplifying assumption that upon decomposition of the organic matter that these cations are bound in, the charge-balance alkalinity will be regenerated (Bijma et al., 2026). Potential losses or transformations of alkalinity due to secondary mineral precipitation in deeper soils or streams are also not accounted for (Clarkson et al., 2024), and the timescale over which full equilibration with ocean conditions occurs remains uncertain and is not explicitly modeled.

330

### 3. Results

#### 3.1 Signal resolvability

A significant increase of 104 ppm (SE: 17) in Ti concentration was observed in treated soils relative to controls ( $p = 0.009$ ), confirming that the applied feedstock signal was statistically resolvable against background variability (Table 2).

335

340



**Table 2. Estimated marginal means ( $\pm$  SE) and contrasts from mixed-effects models comparing treated (T) vs control (C) concentrations (ppm) at the time of sampling for Ti and mobile cations. Differences ( $\Delta$ ) and p-values are based on linear mixed-effects model contrasts.**

Element	Control $\pm$ SE	Treated $\pm$ SE	$\Delta$ (T – C) $\pm$ SE	p value
Ti	1,405 $\pm$ 19	1,509 $\pm$ 18	104 $\pm$ 17	0.009
Mg	639 $\pm$ 34	987 $\pm$ 34	349 $\pm$ 45	-
Ca	3,795 $\pm$ 103	3,994 $\pm$ 103	200 $\pm$ 119	-
K	11,191 $\pm$ 196	11,258 $\pm$ 196	67 $\pm$ 277	-
Na	5,483 $\pm$ 159	5,615 $\pm$ 159	132 $\pm$ 184	-

Observed treated concentrations of Mg were significantly lower than their predicted post-application concentrations under the assumption of no loss ( $p = 0.013$ ), indicating detectable cation depletion consistent with weathering (Table 3). Differences between predicted and observed concentrations for Ca, K, and Na were not statistically significant.

**Table 3. Estimated marginal means ( $\pm$  SE) and contrasts from mixed-effects models comparing predicted post-application (P) vs observed treated (T) concentrations (ppm) for Ti and mobile cations. Differences ( $\Delta$ ) and p-values are based on linear mixed-effects model contrasts.**

Element	Predicted $\pm$ SE	Treated $\pm$ SE	$\Delta$ (P – T) $\pm$ SE	p value
Mg	1,436 $\pm$ 95	987 $\pm$ 95	449 $\pm$ 85	0.013
Ca	4,402 $\pm$ 136	3,994 $\pm$ 136	407 $\pm$ 145	0.068
K	11,651 $\pm$ 195	11,258 $\pm$ 195	393 $\pm$ 151	0.080
Na	5,992 $\pm$ 184	5,615 $\pm$ 184	377 $\pm$ 121	0.052

### 3.2 Dissolution fraction, weathering rate, and inferred GRF application rate

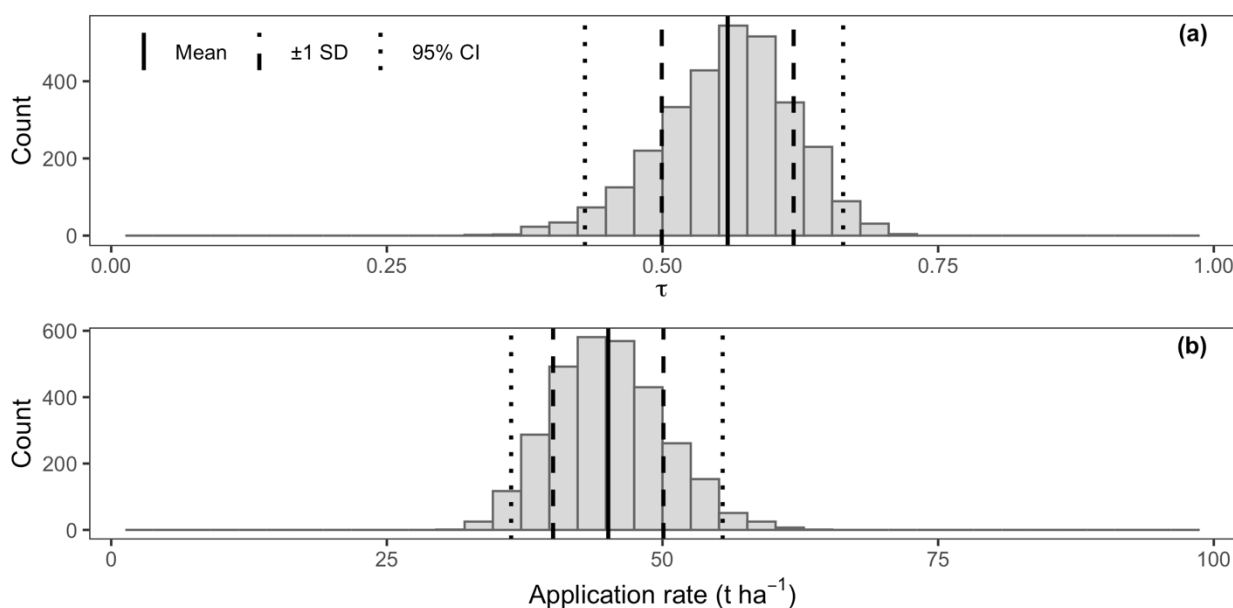
Magnesium yielded a dissolution fraction ( $\tau$ ) of 0.56 (SD: 0.06; 95% CI: 0.43-0.66), representing the most tightly constrained estimate among the measured cations (Table 4, Fig. 1). Sodium yielded a mean  $\tau$  of 0.73 (SD: 0.26; 95% CI: 0.25-1.21), calcium yielded a mean  $\tau$  of 0.67 (SD: 0.14; 95% CI: 0.42-0.99), and potassium yielded a mean  $\tau$  of 0.85 (SD: 0.55; 95% CI: 0.06-2.20). Although the central estimates for Ca, Na, and K were comparable to or greater than the Mg-derived value, their uncertainty intervals were substantially wider, consistent with the fact that the differences between predicted post-application concentrations and observed treated concentrations were not statistically significant.



360

**Table 4. Cation-specific dissolution fraction ( $\tau$ ) and corresponding estimated application rate calculated directly from measured elemental concentrations. Standard deviations (SD) and 95% confidence intervals (CI) were derived from non-parametric bootstrap resampling to quantify uncertainty in the estimates.**

Cation	$\tau \pm \text{SD}$	95% CI	Application Rate (t ha <sup>-1</sup> ) $\pm \text{SD}$	95% CI
Mg	0.56 $\pm$ 0.06	0.43-0.66	44.6 $\pm$ 4.8	35.9-54.3
Ca	0.67 $\pm$ 0.14	0.42-0.99	42.9 $\pm$ 5.2	33.1-53.2
K	0.85 $\pm$ 0.55	0.06-2.20	40.5 $\pm$ 8.2	25.7-57.5
Na	0.73 $\pm$ 0.26	0.25-1.21	42.1 $\pm$ 6.0	31.3-54.6



365

**Figure 1. Bootstrap distributions of the dissolution fraction ( $\tau$ ) and inferred GRF application rate based on Mg and the immobile tracer Ti. Histograms show results from 3,000 hierarchical bootstrap realizations that propagate block-level variability, residual error, and feedstock compositional uncertainty. Solid lines indicate the mean of the bootstrap distribution, dashed lines represent  $\pm 1$  standard deviation, and dotted lines denote the 95% confidence interval bounds.**

370

When expressed as the total positive charge released, calculated by summing the contributions of each cation based on its weathering fraction and normalizing by the total positive charge contained in the applied GRF, approximately 66% of the base-cation charge potential was mobilized over the five-year period. However, because Mg provided the only statistically resolvable signal and the narrowest uncertainty bounds, the Mg-derived dissolution fraction of 56.3% is considered the most robust and conservative estimate of weathering extent. This value is therefore used to calculate the surface-area-normalized weathering rate and to estimate CO<sub>2</sub> uptake. Based on this Mg-derived dissolution fraction and the measured BET surface



area over the five-year period, the corresponding surface-area-normalized weathering rate ( $W_r$ ) is  $1.07 \times 10^{-9} \text{ mol m}^{-2} \text{ s}^{-1}$  (log  
375  $W_r = -8.97$ ).

### 3.3 GRF Application Rate

There was no significant difference in bulk density between the control and treated plots (Table 5). Having been sampled  
shortly after tillage, soil bulk density was unusually low, averaging  $0.61 \text{ g cm}^{-3}$  across the site and indicating that the 0-30  
380 cm sampling depth corresponded to a shallower equivalent mass depth than intended. Using bulk density measurements from  
the subsequent year ( $1.07 \text{ g cm}^{-3}$ ), obtained under more representative conditions, the sampled interval was estimated on an  
equivalent soil mass basis to correspond to approximately the upper 17 cm of the soil profile. The reported plough depth at  
the site was approximately 22 to 25 cm. If  $50 \text{ t ha}^{-1}$  of GRF were uniformly mixed throughout the plough layer,  
approximately 23 to 32% of the applied material would be expected below the sampled interval at the time of sampling.  
Under this assumption, the effective application rate within the sampled layer would range from approximately 34 to  $38.5 \text{ t}$   
385  $\text{ha}^{-1}$ .

The Mg-based application rate inferred through the SOMBA framework was  $44.6 \text{ t ha}^{-1}$ , with a bootstrap-derived standard  
deviation of  $4.8 \text{ t ha}^{-1}$  and a 95% confidence interval of  $35.9\text{-}54.3 \text{ t ha}^{-1}$  (Table 4). Though considered less reliable indicators,  
inferred application rates based on Ca, K, and Na were comparable ( $42.9, 40.5,$  and  $42.1 \text{ t ha}^{-1}$ , respectively).

390 **Table 5. Estimated marginal means ( $\pm$  SE) for control (C) and GRF-treated (T) plots. Differences ( $\Delta$ ) and p-values are based on linear mixed-effects model contrasts.**

	Control $\pm$ SE	Treated $\pm$ SE	$\Delta$ (T - C) $\pm$ SE	p value
pH <sub>H2O</sub>	5.92 $\pm$ 0.05	5.93 $\pm$ 0.05	0.01 $\pm$ 0.07	0.884
Bulk Density ( $\text{g cm}^{-3}$ )	0.60 $\pm$ 0.04	0.61 $\pm$ 0.04	0.01 $\pm$ 0.03	0.674
% POM	0.85 $\pm$ 0.01	0.83 $\pm$ 0.01	-0.01 $\pm$ 0.01	0.084
% MAOM	0.16 $\pm$ 0.01	0.17 $\pm$ 0.01	0.01 $\pm$ 0.01	0.084
<b>% C</b>				
POM	0.25 $\pm$ 0.02	0.29 $\pm$ 0.02	0.04 $\pm$ 0.03	0.232
MAOM	13.9 $\pm$ 0.2	13.6 $\pm$ 0.2	-0.3 $\pm$ 0.2	0.271
SOC	2.52 $\pm$ 0.11	2.76 $\pm$ 0.11	0.24 $\pm$ 0.14	0.172
<b>C (<math>\text{t ha}^{-1}</math>)</b>				
POM	3.87 $\pm$ 0.32	4.37 $\pm$ 0.32	0.50 $\pm$ 0.35	0.249
MAOM	38.7 $\pm$ 2.5	41.6 $\pm$ 2.5	2.9 $\pm$ 1.5	0.156
SOC	45.3 $\pm$ 2.3	50.3 $\pm$ 2.3	5.0 $\pm$ 0.5	0.002



### 3.4 CO<sub>2</sub> Sequestration Estimate

Initial CO<sub>2</sub> uptake via ERW was estimated after accounting for the impact of soil pH on carbonate speciation. Mean soil pH<sub>H<sub>2</sub>O</sub> at the five-year sampling point was 5.94, with no statistically significant difference between treatment and control (Table 5). Likewise, there was no significant difference in pH with treatment after the first growing season, when mean soil pH<sub>H<sub>2</sub>O</sub> was 5.79 (Dietzen and Rosing, 2023).

Laboratory-measured pH values from both time points were recalculated to reflect equilibrium with a plausible range of soil pCO<sub>2</sub> (1,000–40,000 ppm). Under these conditions, estimated in situ soil pH ranged from 4.60 to 5.62. Under these in situ pH and pCO<sub>2</sub> conditions, the fraction of dissolution contributing to bicarbonate generation was estimated to range from 45.1% to 69.2%, corresponding to a soil-solution CO<sub>2</sub> uptake of 3.2–4.9 t CO<sub>2</sub> ha<sup>-1</sup>. Accounting for ocean carbonate equilibration, whereby carbon-capture efficiency evolves toward an upper bound of ~90% (Kanzaki et al., 2023), applying this endpoint conversion factor yields an estimated long-term atmospheric CO<sub>2</sub> reduction of approximately 6.39 t CO<sub>2</sub> ha<sup>-1</sup>.

### 3.5 Soil Organic Carbon

No statistically significant differences were detected in carbon concentration for bulk SOC, POM, or MAOM. Carbon concentrations in treated plots were highly variable but were generally higher than the control for bulk SOC and the POM fraction, whereas MAOM carbon concentrations were lower, consistent with dilution of the fine fraction resulting from the addition of GRF. MAOM comprised 91% of total SOC on average.

In contrast, total SOC stocks were significantly greater in GRF-treated plots compared to controls ( $p = 0.002$ ). Given that bulk density did not differ significantly between treatments, the observed difference in SOC stocks was not attributable to treatment effects on soil mass. Mean SOC stocks increased from 45.3 t C ha<sup>-1</sup> in control plots to 50.3 t C ha<sup>-1</sup> in treated plots, corresponding to an increase of 5.0 t C ha<sup>-1</sup> (equivalent to 18.3 t CO<sub>2</sub> ha<sup>-1</sup>). When expressed as areal carbon stocks, both MAOM and POM exhibited non-significant increases (2.89 t C ha<sup>-1</sup> and 0.5 t C ha<sup>-1</sup>, respectively).

## 4. Discussion

### 4.1 Substantial weathering under temperate field conditions

This five-year field assessment demonstrates substantial dissolution of GRF in temperate agricultural soils, with at least 56 ± 6% of the applied material weathered over this period. The corresponding surface-area-normalized rate of total alkalinity release ( $1.07 \times 10^{-9}$  mol TA m<sup>-2</sup> s<sup>-1</sup>; log  $W_r = -8.97$ ) indicates that rapid silicate weathering can occur in temperate croplands despite lower temperatures and precipitation than tropical regions, where weathering is expected to be fastest (Edwards et al., 2017). Dissolution fractions reported in multi-year agricultural trials of basalt in the U.S. Midwest are broadly comparable to



those observed here, despite differences in feedstock, application frequency, and soil type (Beerling et al., 2024; Kantola et al., 2023).

425 Soil incubation and short-term mesocosm studies typically report surface-area-normalized weathering rates between  $\log W_r = -11$  and  $-12 \text{ mol m}^{-2} \text{ s}^{-1}$  (Kelland et al., 2020; te Pas et al., 2023; Reershemius and Suhrhoff, 2023; Vienne et al., 2024). In contrast, the rate observed here ( $\log W_r = -8.97$ ) is substantially higher and approaches the initial rapid dissolution rate reported for GRF in acidic solution ( $\log W_r \approx -8.6 \text{ mol m}^{-2} \text{ s}^{-1}$ ; Sarkar, 2021). This contrast likely reflects the inability of controlled systems to sustain the mineral-solution disequilibrium that governs weathering rates. At this site, sandy soils with  
430 high hydraulic conductivity and low cation exchange capacity promote rapid flushing of reaction products and maintain chemical disequilibrium, while fluctuating moisture regimes and biological activity further enhance dissolution. The fine particle size distribution and high specific surface area of GRF likely amplify these effects. These results demonstrate that finely ground silicate materials such as GRF can weather rapidly in temperate agricultural fields, emphasizing the role of reactive surface area and hydrological fluxes in sustaining high dissolution rates.

#### 435 **4.2 Implications for MRV**

The substantially higher dissolution fraction inferred using SOMBA relative to earlier exchangeable-cation-based estimates indicates that point measurements may substantially underestimate cumulative weathering. Previously, weathering at this site was estimated at 7.9% over approximately 2.5 years based on repeated measurements of soil exchangeable Mg (Dietzen and Rosing, 2023). In contrast, application of the SOMBA framework yields a dissolution fraction of 56.3% of Mg over five  
440 years. Because silicate weathering rates are generally expected to decline over time as reactive surface area decreases (Brantley, 2025; Power et al., 2025), it is unlikely that accelerated dissolution in later years explains this discrepancy. Rather, the difference suggests that exchangeable Mg measurements did not capture Mg released and subsequently leached during high-precipitation periods. Sampling during the growing season captured transient Mg accumulation under limited leaching but failed to quantify winter losses, leading to substantial underestimation of cumulative dissolution. These results highlight  
445 the importance of time-integrated approaches for MRV, as point measurements of exchangeable cations or pore water may not capture the full flux of weathering products exported from the soil system.

Not all cations provided equally robust constraints on dissolution. Only Mg showed statistically significant differences between predicted and observed treated concentrations, whereas Ca, Na, and K exhibited wider uncertainty intervals due to  
450 larger and more heterogeneous background soil pools (Suhrhoff et al., 2024). Background concentrations of Ca and Na were approximately one order of magnitude greater than those of Mg, while K concentrations were roughly two orders of magnitude greater than Mg, with correspondingly higher spatial variability. This elevated background variability reduced sensitivity to treatment-induced changes. Consequently, the Mg-based weathering fraction represents the most defensible single-element estimate and can be considered conservative, as dissolution fractions inferred for other cations were



455 consistently higher. Despite these differences in precision, dissolution fractions were broadly consistent across base cations, supporting the overall magnitude of weathering inferred from SOMBA.

These results highlight that background soil variability imposes a fundamental constraint on the detectability of weathering signals in field settings (Rogers and Maher, 2026; Suhrhoff et al., 2024) but also demonstrate that this limitation can be mitigated through careful experimental design. Application rates derived from SOMBA were consistent with the estimated mass of GRF present within the sampled soil layer, with the 95% confidence intervals of the inferred rates overlapping this estimate across all elements. This agreement reflects favorable experimental conditions, including repeated ploughing that promoted thorough mixing of the feedstock within the plough layer and a randomized block design that accounted for within-field heterogeneity, a key challenge for soil mass balance approaches (Rogers and Maher, 2026). Together, these factors enabled a sufficiently clear geochemical signal to constrain dissolution despite large background pools.

In less controlled settings, incomplete mixing and greater spatial heterogeneity are likely to obscure treatment signals and increase uncertainty in SOMBA-derived estimates. These challenges may be particularly pronounced in shorter-duration studies with incomplete mixing via repeated tillage or when experimental designs do not explicitly account for background variability. While randomized block designs may be impractical for commercial deployments, experimental field trials aimed at evaluating ERW should incorporate these principles wherever possible. In commercial applications, although there may be incentives to quantify weathering rapidly for crediting purposes, allowing more time for tillage to homogenize the amendment within the plough layer may ultimately produce clearer geochemical signals and reduce the analytical effort required to detect weathering.

475 The substantially higher dissolution fraction inferred from SOMBA also implies a major upward revision of estimated CO<sub>2</sub> uptake relative to the previously reported estimate of 728 kg CO<sub>2</sub> ha<sup>-1</sup> in Dietzen & Rosing (2023). In the present analysis, cumulative dissolution is estimated at approximately 56% after five years, corresponding to initial CO<sub>2</sub> uptake of 3.2–4.9 t CO<sub>2</sub> ha<sup>-1</sup>, depending on carbonate speciation in the soil solution. Even at the lower bound, this represents an approximately fivefold increase relative to the previous estimate.

Separately, we estimated the long-term atmospheric CO<sub>2</sub> removal, which depends on the export of net charge-balance alkalinity from the terrestrial system and its subsequent equilibration with ocean carbonate chemistry. Applying a representative present-day ocean buffering efficiency of 90% (Kanzaki et al., 2023) yields an estimated atmospheric CO<sub>2</sub> removal of approximately 6.39 t CO<sub>2</sub> ha<sup>-1</sup>. At the Vojens site, equilibration with ocean carbonate chemistry is expected to occur on relatively short timescales due to the local hydrological setting. The field is located on permeable sandy outwash deposits with a shallow water table and strong hydrological connectivity to the stream network (Klimadatastyrelsen, 2026), conditions that favor rapid transport of dissolved weathering products from the soil to surface waters and ultimately the



490 coastal ocean. As a result, alkalinity generated by weathering is likely to reach the ocean and equilibrate within a relatively short period, potentially supporting the application of the ocean correction factor instead of the initial soil solution-based correction factor when estimating CDR from this site.

### 4.3 Organic Carbon Dynamics

In addition to inorganic carbon removal, GRF application was associated with a significant increase in SOC stocks of 5.0 t C ha<sup>-1</sup>, equivalent to the storage of an additional 18.3 t CO<sub>2</sub> ha<sup>-1</sup> in soil carbon pools. In contrast, SOC concentrations did not differ significantly between treatments, and bulk density was likewise not significantly affected when analyzed independently. Because SOC stocks integrate both carbon concentration and bulk density, which are often inversely related, expressing SOC on an area basis reduced residual variance and revealed a consistent treatment effect on carbon stocks.

500 Notably, this organic carbon increase exceeds the maximum theoretical CO<sub>2</sub> uptake achievable through full dissolution of the GRF and is more than double the CO<sub>2</sub> uptake inferred from the observed dissolution fraction. These findings indicate that organic carbon dynamics may represent a substantial component of the total climate impact of GRF application. This observation is consistent with growing evidence that organic carbon responses can represent a major component of the climate benefit associated with ERW, in some cases exceeding inorganic carbon sequestration through alkalinity generation (Anthony et al., 2025; Vicca et al., 2022; Xu et al., 2024).

505 Reported responses of SOC to mineral amendments vary widely across studies, reflecting strong context dependency related to soil properties, climate, plant communities, and experimental duration. Several studies report initial losses of soil organic matter following mineral additions, often attributed to stimulated microbial activity and accelerated decomposition of existing mineral-associated organic matter pools (Boito et al., 2025; Fang et al., 2023; Niron et al., 2024; Sokol et al., 2024). However, longer-term observations (Sohng et al., 2025; Sokol et al., 2024; Steinwidder et al., 2025) and meta-analyses of the effects of liming (Wang et al., 2021; Zhang et al., 2022) suggest that these early losses may represent transient responses, with systems transitioning toward net SOC accumulation after one to several years as stabilization processes and increased carbon inputs begin to dominate. Similar temporal dynamics have been reported following agricultural liming, where increased microbial activity can initially stimulate organic matter mineralization but longer-term improvements in soil fertility and plant productivity increase carbon inputs and ultimately promote SOC accumulation (Paradelo et al., 2015). Our five-year observations are consistent with this longer-term phase in which stabilization processes outweigh early-stage decomposition.

520 Although increases in POM and MAOM carbon stocks were not statistically significant individually, the majority of SOC gains were associated with the mineral-associated fraction, which comprises over 90% of total SOC at this site. This pattern is consistent with mechanisms proposed for ERW systems in which mineral additions increase reactive surface area for

organo-mineral interactions and promote the stabilization of organic carbon and observed results in other trials (Niron et al., 2024; Ramos et al., 2024; Steinwider et al., 2025; Xu et al., 2024). The effect may be particularly pronounced in coarse-textured sandy soils such as the one studied here, where mineral surface area for organic matter stabilization is initially limited. In the case of GRF, the high surface area of the applied material itself may provide abundant reactive mineral surfaces capable of facilitating MAOM formation from the time of application. The predominance of SOC gains within the mineral-associated fraction suggests that stabilization processes ultimately outweighed potential short-term increases in rhizosphere respiration that can temporarily enhance organic matter decomposition (Boito et al., 2025; Steinwider et al., 2025).

530

Assessing SOC responses in this sandy context provides insight into how ERW may alter carbon stabilization pathways in soils that are initially limited in reactive mineral surfaces (Georgiou et al., 2022; Slessarev et al., 2022). These findings indicate that ERW can contribute to climate mitigation not only through inorganic carbon sequestration but also by promoting organic carbon stabilization in agricultural soils, highlighting the importance of incorporating SOC dynamics into ERW monitoring and verification frameworks. Beyond carbon sequestration, increases in SOC are associated with improved soil structure, nutrient retention, and water-holding capacity, suggesting potential co-benefits for agricultural sustainability.

535

#### 4.4 Potential for GRF Application in Denmark

Extrapolating the results of the present field trial to the broader Danish agricultural context suggests a substantial CDR potential for ERW on sandy soils in Western Denmark. Denmark has approximately 2.6 million hectares of utilized agricultural area, of which an estimated 31%, roughly 807,000 ha, is classified as sandy soils broadly comparable to the Vojens field site (Cropland, 2026; Styczen and Sørensen, 2004). Applying the trial application rate of 50 t ha<sup>-1</sup> across this area would correspond to a total application of approximately 40 million tons of feedstock.

540

In the sandy outwash regions of western Jutland, the low-relief topography, permeable glacial sediments, and dense surface water network result in widespread groundwater-surface water connectivity (Duque et al., 2023). These hydrological conditions suggest that alkalinity generated through mineral weathering in these soils is likely to be transported through shallow groundwater systems to streams and ultimately to coastal waters within a relatively short timescale, potentially supporting the use of an ocean equilibration correction when estimating net CDR, though hydrologic modelling is needed to evaluate the validity of this simplification for the region.

545

Assuming that the five-year dissolution fraction observed at the Vojens site (56%) is representative of comparable sandy soils across Denmark and applying a 0.9 ocean-equilibration correction (Kanzaki et al., 2023), over 5 years a single application of GRF at this rate across Denmark's sandy agricultural soils would yield an estimated net CDR potential of

550



555 approximately 5.1 million tons of CO<sub>2</sub>, equalling almost half the total annual greenhouse gas emissions from Danish agriculture in CO<sub>2</sub> equivalents (Albrektsen and Mikkelsen, 2026).

## Conclusion

560 This five-year field experiment provides rare, time-integrated constraints on ERW under temperate agricultural conditions. Using a soil mass balance framework within a randomized block design, we estimate that approximately 56% of the applied glacial rock flour dissolved over five years. These results demonstrate that finely grained silicate materials can undergo substantial dissolution in well-drained sandy soils, highlighting the importance of hydrological flushing and reactive surface area in maintaining mineral–solution disequilibrium under field conditions.

565 Accounting for carbonate system constraints under realistic soil pCO<sub>2</sub> conditions, this degree of dissolution corresponds to an initial inorganic CO<sub>2</sub> uptake of 3.2–4.9 t CO<sub>2</sub> ha<sup>-1</sup>, with a projected long-term atmospheric removal of up to 6.39 t CO<sub>2</sub> ha<sup>-1</sup> following alkalinity export and equilibration with ocean carbonate chemistry. These estimates substantially exceed earlier site-specific assessments based on exchangeable cation measurements, indicating that point measurements can underestimate cumulative weathering and reinforcing the need for time-integrated approaches for MRV.

570 In parallel, GRF application resulted in a significant increase in soil organic carbon stocks of 5.0 t C ha<sup>-1</sup> (18.3 t CO<sub>2</sub> ha<sup>-1</sup>). Although the mechanisms cannot be uniquely resolved, the predominance of gains in the mineral-associated fraction is consistent with enhanced organo-mineral stabilization in this coarse-textured soil. The magnitude of this response indicates that organic carbon dynamics may represent a substantial component of the climate impact of ERW.

575 Together, these findings provide field-based evidence that ERW of glacial rock flour can drive substantial carbon sequestration through both inorganic and organic pathways over multi-year timescales. More broadly, the results highlight the importance of combining time-integrated geochemical methods with soil carbon measurements to constrain the full carbon balance of enhanced weathering systems and support the development of robust, field-deployable MRV frameworks for agricultural carbon removal.

580



### Code and data availability

Soil and feedstock data, R code, and the updated carbon-capture efficiency calculator can be accessed at:

<https://doi.org/10.17894/ucph.63ae53e9-9269-4021-8f25-084dcbdf9459>

### Author contributions

585 Conceptualization: MTR, CD; methodology: CD, MR, TJS; formal analysis: CD; investigation: CD and MR; writing-  
original draft: CD and MR; writing review & editing: CD, MR, TJS, and MTR; visualization: CD and TJS; supervision:  
MTR; project administration: CD; funding acquisition, MTR.

### Competing interests

590 Minik Thorleif Rosing is Chairman of the Board for the Rock Flour Company, a Danish Start-up company aiming at  
developing glacial rock flour for climate change mitigation and global food security. Christiana Dietzen acts as a scientific  
advisor to the company. Neither receive financial compensation for these roles, but Rosing has invested personal equity for  
starting the company. The Rock Flour Company has not influenced the study and has no commercial interests in the research  
reported here. The remaining authors have no relevant financial or non-financial interests to disclose.

### Disclaimer

595 Copernicus Publications remains neutral with regard to jurisdictional claims made in the text, published maps, institutional  
affiliations, or any other geographical representation in this paper. While Copernicus Publications makes every effort to  
include appropriate place names, the final responsibility lies with the authors. Views expressed in the text are those of the  
authors and do not necessarily reflect the views of the publisher.

### Acknowledgements

600 The authors would like to thank the Novo Nordisk Foundation for funding this research. We would also like to acknowledge  
Lars Stoumann Jensen and Klara Cecilia Gunnarsen, who designed and organized the installation of the field trial, the farmer  
Flemming Skov, and the personnel at SEGES (National agricultural knowledge and innovation center) and SLF (Sønderjysk  
Landboforening), who managed the site for the first three years of the experiment. Claude and ChatGPT were used to assist  
in converting the Python implementation of the SOMBA framework published in Suhrhoff et al. (2025) into R code and in  
605 modifying the framework to incorporate the use of a randomized block design.



## Financial support

This work was funded by the Novo Nordisk Foundation (grant number: NNF22SA0079616).

## References

- Albrektsen, R. and Mikkelsen, M. H.: Danish Emission Inventories for Agriculture. Inventories 1985 - 2023, DCE - Danish Centre for Environment and Energy, 2026.
- 610 Klimadatastyrelsen: <https://hipdata.dk/>, last access: 18 March 2026.
- Anthony, T. L., Jones, A. R., and Silver, W. L.: Supplementing Enhanced Weathering With Organic Amendments Accelerates the Net Climate Benefit of Soil Amendments in Rangeland Soils, *AGU Advances*, 6, e2024AV001480, <https://doi.org/10.1029/2024AV001480>, 2025.
- 615 Basile-Doelsch, I., Balesdent, J., and Pellerin, S.: Reviews and syntheses: The mechanisms underlying carbon storage in soil, *Biogeosciences*, 17, 5223–5242, <https://doi.org/10.5194/bg-17-5223-2020>, 2020.
- Beerling, D. J., Leake, J. R., Long, S. P., Scholes, J. D., Ton, J., Nelson, P. N., Bird, M., Kantzas, E., Taylor, L. L., Sarkar, B., Kelland, M., DeLucia, E., Kantola, I., Müller, C., Rau, G., and Hansen, J.: Farming with crops and rocks to address global climate, food and soil security, *Nature Plants*, 4, <https://doi.org/10.1038/s41477-018-0108-y>, 2018.
- 620 Beerling, D. J., Epihov, D. Z., Kantola, I. B., Masters, M. D., Reershemius, T., Planavsky, N. J., Reinhard, C. T., Jordan, J. S., Thorne, S. J., Weber, J., Val Martin, M., Freckleton, R. P., Hartley, S. E., James, R. H., Pearce, C. R., DeLucia, E. H., and Banwart, S. A.: Enhanced weathering in the US Corn Belt delivers carbon removal with agronomic benefits, *Proceedings of the National Academy of Sciences*, 121, e2319436121, <https://doi.org/10.1073/pnas.2319436121>, 2024.
- 625 Beerling, D. J., Reinhard, C. T., James, R. H., Khan, A., Pidgeon, N., and Planavsky, N. J.: Challenges and opportunities in scaling enhanced weathering for carbon dioxide removal, *Nat Rev Earth Environ*, 6, 672–686, <https://doi.org/10.1038/s43017-025-00713-7>, 2025.
- Bertagni, M. B. and Porporato, A.: The Carbon-Capture Efficiency of Natural Water Alkalinization: Implications For Enhanced weathering, *Science of The Total Environment*, 838, 156524, <https://doi.org/10.1016/j.scitotenv.2022.156524>, 2022.
- 630 Bijma, J., Hagens, M., Hammes, J. S., Planavsky, N., Pogge von Strandmann, P. A. E., Reershemius, T., Reinhard, C. T., Renforth, P., Suhrhoff, T. J., Vicca, S., Vienne, A., and Wolf-Gladrow, D.: Reviews and syntheses: Carbon vs. cation based MRV of Enhanced Rock Weathering and the issue of soil organic carbon, *Biogeosciences*, 23, 53–75, <https://doi.org/10.5194/bg-23-53-2026>, 2026.
- 635 Boito, L., Steinwider, L., Rijnders, J., Berwouts, J., Janse, S., Niron, H., Roussard, J., Vienne, A., and Vicca, S.: Enhanced Rock Weathering Altered Soil Organic Carbon Fluxes in a Plant Trial, *Global Change Biology*, 31, e70373, <https://doi.org/10.1111/gcb.70373>, 2025.
- Brantley, S. L.: Understanding the Lab-Field Discrepancy in Mineral Dissolution From Flasks to Enhanced Rock Weathering, *Reviews of Geophysics*, 63, e2025RG000881, <https://doi.org/10.1029/2025RG000881>, 2025.



- 640 Buma, B., Dietzen, C., Gordon, D. R., Maher, K., Neumann, R. B., Planavsky, N. J., Reershemius, T., Suhrhoff, T. J., Vicca, S., Waring, B. G., Almaraz, M., Calabrese, S., Derry, L. A., Morgan, M. G., Higgins, J., Houlton, B. Z., Kanzaki, Y., Klemme, A., Kukla, T., Oldfield, E. E., Power, I. M., Pearce, C. R., Silver, W. L., and Zhang, S.: Expert elicitation on agricultural enhanced weathering reveals carbon dioxide removal potential and uncertainties in loss pathways, *Commun Earth Environ*, <https://doi.org/10.1038/s43247-026-03375-5>, 2026.
- 645 Calabrese, S., Wild, B., Bertagni, M. B., Bourg, I. C., White, C., Aburto, F., Cipolla, G., Noto, L. V., and Porporato, A.: Nano- to Global-Scale Uncertainties in Terrestrial Enhanced Weathering, *Environmental Science & Technology*, 12, 2021.
- Cambardella, C. A. and Elliott, E. T.: Particulate Soil Organic-Matter Changes across a Grassland Cultivation Sequence, *Soil Science Soc of Amer J*, 56, 777–783, <https://doi.org/10.2136/sssaj1992.03615995005600030017x>, 1992.
- 650 Carignan, J., Hild, P., Mevelle, G., Morel, J., and Yeghicheyan, D.: Routine Analyses of Trace Elements in Geological Samples using Flow Injection and Low Pressure On-Line Liquid Chromatography Coupled to ICP-MS: A Study of Geochemical Reference Materials BR, DR-N, UB-N, AN-G and GH, *Geostandards and Geoanalytical Research*, 25, 187–198, <https://doi.org/10.1111/j.1751-908X.2001.tb00595.x>, 2001.
- Clarkson, M. O., Larkin, C. S., Swoboda, P., Reershemius, T., Suhrhoff, T. J., Maesano, C. N., and Campbell, J. S.: A review of measurement for quantification of carbon dioxide removal by enhanced weathering in soil, *Front. Clim.*, 6, <https://doi.org/10.3389/fclim.2024.1345224>, 2024.
- 655 Dietzen, C. and Rosing, M. T.: Quantification of CO<sub>2</sub> uptake by enhanced weathering of silicate minerals applied to acidic soils, *International Journal of Greenhouse Gas Control*, 125, 103872, <https://doi.org/10.1016/j.ijggc.2023.103872>, 2023.
- Dietzen, C., Gunnarsen, K. C., Jensen, L. S., and Rosing, M. T.: Glacial Rock Flour Field Trial: Vojens, Denmark [Data set], University of Copenhagen, <https://doi.org/https://doi.org/10.17894/UCPH.16FBF798-6DE6-40D6-8437-E70CD0A42FC1>, 2022.
- 660 Dietzen, C., Rizzi, M., Suhrhoff, T. J., and Rosing, M.: 5 year resampling of soil from Glacial Rock Flour Field trial in Vojens DK: Data and code for analysis, <https://doi.org/https://doi.org/10.17894/ucph.63ae53e9-9269-4021-8f25-084dcbdf9459>, 2026.
- Vejrarkiv: <http://www.dmi.dk/vejrarkiv/>, last access: 18 March 2026.
- 665 Dupla, X., Bertagni, M. B., and Grand, S.: Three Years of Field Trials Indicate a Sustained Enhanced Rock Weathering Signal with Limited CO<sub>2</sub> Removal, *Environ. Sci. Technol.*, 59, 25751–25764, <https://doi.org/10.1021/acs.est.5c09820>, 2025.
- Duque, C., Nilsson, B., and Engesgaard, P.: Groundwater–surface water interaction in Denmark, *WIREs Water*, 10, e1664, <https://doi.org/10.1002/wat2.1664>, 2023.
- 670 Edwards, D. P., Lim, F., James, R. H., Pearce, C. R., Scholes, J., Freckleton, R. P., Beerling, D. J., and Edwards, D. P.: Climate change mitigation: potential benefits and pitfalls of enhanced rock weathering in tropical agriculture, *Biology Letters*, 13, <https://doi.org/10.1098/rsbl.2016.0715>, 2017.
- Elberling, B. and Matthiesen, H.: Methodologically controlled variations in laboratory and field pH measurements in waterlogged soils, *European Journal of Soil Science*, 58, 207–214, <https://doi.org/10.1111/j.1365-2389.2006.00828.x>, 2007.
- 675 Fang, Q., Lu, A., Hong, H., Kuzyakov, Y., Algeo, T. J., Zhao, L., Olshansky, Y., Moravec, B., Barrientes, D. M., and Chorover, J.: Mineral weathering is linked to microbial priming in the critical zone, *Nat Commun*, 14, 345, <https://doi.org/10.1038/s41467-022-35671-x>, 2023.



- Georgiou, K., Jackson, R. B., Vinduškova, O., Abramoff, R. Z., Ahlström, A., Feng, W., Harden, J. W., Pellegrini, A. F. A., Polley, H. W., Soong, J. L., Riley, W. J., and Torn, M. S.: Global stocks and capacity of mineral-associated soil organic carbon, *Nat Commun*, 13, 3797, <https://doi.org/10.1038/s41467-022-31540-9>, 2022.
- 680 Georgiou, K., Angers, D., Champiny, R. E., Cotrufo, M. F., Craig, M. E., Doetterl, S., Grandy, A. S., Lavalley, J. M., Lin, Y., Lugato, E., Poeplau, C., Rocci, K. S., Schweizer, S. A., Six, J., and Wieder, W. R.: Soil Carbon Saturation: What Do We Really Know?, *Glob Chang Biol*, 31, e70197, <https://doi.org/10.1111/gcb.70197>, 2025.
- Surface Geology Map of Denmark 1:25.000: <https://eng.geus.dk/products-services-facilities/data-and-maps/maps-of-denmark>, last access: 3 November 2022.
- 685 Gunnarsen, K. C., Jensen, L. S., Rosing, M. T., and Dietzen, C.: Greenlandic Glacial Rock Flour Improves Crop Yield in Organic Agricultural Production, *Nutrient Cycling in Agroecosystems*, 2023.
- Hartmann, J., West, A. J., Renforth, P., Köhler, P., De La Rocha, C. L., Wolf-gladrow, D. A., Dürr, H. H., Scheffran, J., Rocha, C. L. D. L., Wolf-gladrow, D. A., Dürr, H. H., Scheffran, J., De La Rocha, C. L., Wolf-gladrow, D. A., Dürr, H. H., and Scheffran, J.: Enhanced chemical weathering as a geoengineering strategy to reduce atmospheric carbon dioxide, supply nutrients, and mitigate ocean acidification, *Reviews of Geophysics*, 51, 113–149, <https://doi.org/10.1002/rog.20004>, 2013.
- 690 Holden, F., Davies, K., Bird, M., Hume, R., Green, H., Beerling, D., and Nelson, P.: In-field carbon dioxide removal via weathering of crushed basalt applied to acidic tropical agricultural soil, *Science of The Total Environment*, 955, 176568, <https://doi.org/10.1016/j.scitotenv.2024.176568>, 2024.
- Huang, J. and Hartemink, A. E.: Soil and environmental issues in sandy soils, *Earth-Science Reviews*, 208, 103295, <https://doi.org/10.1016/j.earscirev.2020.103295>, 2020.
- 695 Kantola, I. B., Blanc-Betes, E., Masters, M. D., Chang, E., Marklein, A., Moore, C. E., von Haden, A., Bernacchi, C. J., Wolf, A., Epihov, D. Z., Beerling, D. J., and DeLucia, E. H.: Improved net carbon budgets in the US Midwest through direct measured impacts of enhanced weathering, *Global Change Biology*, 29, 7012–7028, <https://doi.org/10.1111/gcb.16903>, 2023.
- 700 Kanzaki, Y., Planavsky, N. J., and Reinhard, C. T.: New estimates of the storage permanence and ocean co-benefits of enhanced rock weathering, *PNAS Nexus*, 2, pgad059, <https://doi.org/10.1093/pnasnexus/pgad059>, 2023.
- Kelland, M. E., Wade, P. W., Lewis, A. L., Taylor, L. L., Sarkar, B., Andrews, M. G., Lomas, M. R., Cotton, T. E. A. E. A., Kemp, S. J., James, R. H., Pearce, C. R., Hartley, S. E., Hodson, M. E., Leake, J. R., Banwart, S. A., Beerling, D. J., Wade, P. W., Johnson, D. A., Lewis, A. L., Andrews, M. G., Lomas, M. R., Cotton, T. E. A. E. A., Kemp, S. J., Taylor, L. L., James, R. H., Pearce, C. R., Hartley, S. E., Hodson, M. E., Leake, J. R., Banwart, S. A., Beerling, D. J., Sarkar, B., Andrews, M. G., Lomas, M. R., Cotton, T. E. A. E. A., Kemp, S. J., James, R. H., Pearce, C. R., Hartley, S. E., Hodson, M. E., Leake, J. R., Banwart, S. A., and Beerling, D. J.: Increased yield and CO<sub>2</sub> sequestration potential with the C<sub>4</sub> cereal Sorghum bicolor cultivated in basaltic rock dust-amended agricultural soil, *Global Change Biology*, 26, 3658–3676, <https://doi.org/10.1111/gcb.15089>, 2020.
- 710 Kleber, M., Bourg, I. C., Coward, E. K., Hansel, C. M., Myneni, S. C. B., and Nunan, N.: Dynamic interactions at the mineral–organic matter interface, *Nat Rev Earth Environ*, 2, 402–421, <https://doi.org/10.1038/s43017-021-00162-y>, 2021.
- Köhler, P., Hartmann, J., and Wolf-Gladrow, D. A.: Geoengineering potential of artificially enhanced silicate weathering of olivine., *Proceedings of the National Academy of Sciences of the United States of America*, 107, 20228–20233, <https://doi.org/10.1073/pnas.1000545107>, 2010.



- 715 Larkin, C. S., Andrews, M. G., Pearce, C. R., Yeong, K. L., Beerling, D. J., Bellamy, J., Benedick, S., Freckleton, R. P., Goring-Harford, H., Sadekar, S., and James, R. H.: Quantification of CO<sub>2</sub> removal in a large-scale enhanced weathering field trial on an oil palm plantation in Sabah, Malaysia, *Front. Clim.*, 4, <https://doi.org/10.3389/fclim.2022.959229>, 2022.
- Lenth, R.: emmeans: Estimated Marginal Means, aka Least-Squares Means., 2022.
- 720 Lopez-Sangil, L. and Rovira, P.: Sequential chemical extractions of the mineral-associated soil organic matter: An integrated approach for the fractionation of organo-mineral complexes, *Soil Biology and Biochemistry*, 62, 57–67, <https://doi.org/10.1016/j.soilbio.2013.03.004>, 2013.
- Matthiesen, H.: In situ measurement of soil pH, *Journal of Archaeological Science*, 31, 1373–1381, <https://doi.org/10.1016/j.jas.2004.03.005>, 2004.
- 725 Niron, H., Vienne, A., Frings, P., Poetra, R., and Vicca, S.: Exploring the synergy of enhanced weathering and *Bacillus subtilis*: A promising strategy for sustainable agriculture, *Global Change Biology*, 30, e17511, <https://doi.org/10.1111/gcb.17511>, 2024.
- Obour, P. B., Dietzen, C., Opong Danso, E., Arthur, E., Adu, M. O., and Rosing, M. T.: Limited short-term benefits of glacial rock flour for enhancing the physical quality of tropical arable soils, *European Journal of Soil Science*, 75, e70028, <https://doi.org/10.1111/ejss.70028>, 2024.
- 730 Opong Danso, E., Dietzen, C., Arthur, E., and Rosing, M. T.: Enduring increases in maize yield are a co-benefit of enhanced weathering of Greenlandic glacial rock flour in Ghana, *Nutr Cycl Agroecosyst*, 131, 761–772, <https://doi.org/10.1007/s10705-025-10442-4>, 2025.
- Paradelo, R., Virto, I., and Chenu, C.: Agriculture, Ecosystems and Environment Net effect of liming on soil organic carbon stocks: A review, *Agriculture, Ecosystems and Environment*, 202, 98–107, <https://doi.org/10.1016/j.agee.2015.01.005>, 2015.
- 735 te Pas, E. E. E. M., Hagens, M., and Comans, R. N. J.: Assessment of the enhanced weathering potential of different silicate minerals to improve soil quality and sequester CO<sub>2</sub>, *Frontiers in Climate*, 4, 954064, <https://doi.org/10.3389/fclim.2022.954064>, 2023.
- Pinheiro, J., Bates, D., DebRoy, S., Sarkar, D., and R Core Team: nlme: Linear and Nonlinear Mixed Effects Models, 2017.
- 740 Power, I. M., Hatten, V. N. J., Guo, M., Schaffer, Z. R., Rausis, K., and Klyn-Hesselink, H.: Are enhanced rock weathering rates overestimated? A few geochemical and mineralogical pitfalls, *Front. Clim.*, 6, <https://doi.org/10.3389/fclim.2024.1510747>, 2025.
- R Core Team: R: A Language and Environment for Statistical Computing, 2023.
- 745 Ramos, E. J., Larsen, W. J., Hou, Y., Muñoz, S., Kemeny, P. C., Scheingross, J. S., Repasch, M. N., Hovius, N., Sachse, D., Ibarra, D. E., and Torres, M. A.: Competition or collaboration: Clay formation sets the relationship between silicate weathering and organic carbon burial in soil, *Earth and Planetary Science Letters*, 628, 118584, <https://doi.org/10.1016/j.epsl.2024.118584>, 2024.
- Reershemius, T. and Suhrhoff, T. J.: On error, uncertainty, and assumptions in calculating carbon dioxide removal rates by enhanced rock weathering in Kantola et al., 2023, *Global Change Biology*, 30, <https://doi.org/10.1111/gcb.17025>, 2023.
- Reershemius, T., Kelland, M. E., Jordan, J. S., Davis, I. R., D’Ascanio, R., Kalderon-Asael, B., Asael, D., Suhrhoff, T. J., Epihov, D. Z., Beerling, D. J., Reinhard, C. T., and Planavsky, N. J.: Initial Validation of a Soil-Based Mass-Balance



- 750 Approach for Empirical Monitoring of Enhanced Rock Weathering Rates, *Environ. Sci. Technol.*, <https://doi.org/10.1021/acs.est.3c03609>, 2023.
- Renforth, P. and Henderson, G.: Assessing ocean alkalinity for carbon sequestration, *Reviews of Geophysics*, 55, 636–674, <https://doi.org/10.1002/2016RG000533>, 2017.
- 755 Rogers, B. and Maher, K.: An uncertainty-aware framework for solid-phase measurement and verification of enhanced weathering, *Front. Clim.*, 7, <https://doi.org/10.3389/fclim.2025.1688361>, 2026.
- Sanderman, J., Fillery, I. R. P., Jongepier, R., Massalsky, A., Roper, M. M., Macdonald, L. M., Maddern, T., Murphy, D. V., and Baldock, J. A.: Carbon sequestration under subtropical perennial pastures II: Carbon dynamics, *Soil Research*, 51, 771–780, <https://doi.org/10.1071/SR12351>, 2013.
- 760 Sarkar, S. R.: Glacial Rock Flour: its Characteristics and Enhanced Weathering, PhD Thesis, University of Copenhagen, 2021.
- Six, J., Conant, R. T., Paul, E. A., and Paustian, K.: Stabilization mechanisms of soil organic matter: Implications for C-saturation of soils, *Plant and Soil*, 241, 155–176, <https://doi.org/10.1023/A:1016125726789>, 2002.
- 765 Slessarev, E. W., Chadwick, O. A., Sokol, N. W., Nuccio, E. E., and Pett-Ridge, J.: Rock weathering controls the potential for soil carbon storage at a continental scale, *Biogeochemistry*, 157, 1–13, <https://doi.org/10.1007/s10533-021-00859-8>, 2022.
- Sohng, J., Sokol, N. W., Whiteaker, S., Schmidt, R., Holzer, I., Goertzen, H., Peña, J., Houlton, B. Z., Montañez, I., O’Geen, A., and Scow, K.: Combining organic amendments with enhanced rock weathering shifts soil carbon storage in croplands, *Science of The Total Environment*, 998, 180179, <https://doi.org/10.1016/j.scitotenv.2025.180179>, 2025.
- 770 Sokol, N. W., Sohng, J., Moreland, K., Slessarev, E., Goertzen, H., Schmidt, R., Samaddar, S., Holzer, I., Almaraz, M., Geoghegan, E., Houlton, B., Montañez, I., Pett-Ridge, J., and Scow, K.: Reduced accrual of mineral-associated organic matter after two years of enhanced rock weathering in cropland soils, though no net losses of soil organic carbon, *Biogeochemistry*, 167, 989–1005, <https://doi.org/10.1007/s10533-024-01160-0>, 2024.
- Cropland: <https://www.dst.dk/en/Statistik/emner/erhvervsliv/landbrug-gartneri-og-skovbrug/det-dyrkede-areal>, last access: 18 March 2026.
- 775 Steinwider, L., Boito, L., Frings, P. J., Niron, H., Rijnders, J., de Schutter, A., Vienne, A., and Vicca, S.: Beyond Inorganic C: Soil Organic C as a Key Pathway for Carbon Sequestration in Enhanced Weathering, *Global Change Biology*, 31, e70340, <https://doi.org/10.1111/gcb.70340>, 2025.
- Styczen, M. and Sørensen, P. B.: Scenarios and Model Describing Fate and Transport of Pesticides in Surface Water for Danish Conditions, Danish Environmental Protection Agency, 2004.
- 780 Suhrhoff, T. J., Reershemius, T., Wang, J., Jordan, J. S., Reinhard, C. T., and Planavsky, N. J.: A tool for assessing the sensitivity of soil-based approaches for quantifying enhanced weathering: a US case study, *Front. Clim.*, 6, <https://doi.org/10.3389/fclim.2024.1346117>, 2024.
- 785 Suhrhoff, T. J., Reershemius, T., Jordan, J. S., Li, S., Zhang, S., Milliken, E., Kalderon-Asael, B., Ebert, Y., Nyateka, R., Thompson, J. T., Reinhard, C. T., and Planavsky, N. J.: An Updated Framework and Signal-to-Noise Analysis of Soil Mass Balance Approaches for Quantifying Enhanced Weathering on Managed Lands, *Environ. Sci. Technol.*, *acs.est.5c08303*, <https://doi.org/10.1021/acs.est.5c08303>, 2025.



- 790 Tingey, S., Wadham, J. L., Telling, J., Flynn, S., Hawkings, J. R., Palinkas, S. S., Mun, Y., Yates, C. A., Lamarche-Gagnon, G., Burford, R., Ramanathan, A. L., Hetherington, A., Dodd, A. N., Liu, X., and Sgouridis, F.: The potential for glacial flour to impact soil fertility, crop yield and nutrition in mountain regions, *iScience*, 28, <https://doi.org/10.1016/j.isci.2024.111476>, 2025.
- Vicca, S., Goll, D. S., Hagens, M., Hartmann, J., Janssens, I. A., Neubeck, A., Peñuelas, J., Poblador, S., Rijnders, J., Sardans, J., Struyf, E., Swoboda, P., Groenigen, J. W., Vienne, A., and Verbruggen, E.: Is the climate change mitigation effect of enhanced silicate weathering governed by biological processes?, *Global Change Biology*, 28, 711–726, <https://doi.org/10.1111/gcb.15993>, 2022.
- 795 Vienne, A., Frings, P., Poblador, S., Steinwider, L., Rijnders, J., Schoelynck, J., Vinduskova, O., and Vicca, S.: Earthworms in an enhanced weathering mesocosm experiment: Effects on soil carbon sequestration, base cation exchange and soil CO<sub>2</sub> efflux, *Soil Biology and Biochemistry*, 199, 109596, <https://doi.org/10.1016/j.soilbio.2024.109596>, 2024.
- 800 Wang, Y., Yao, Z., Zhan, Y., Zheng, X., Zhou, M., Yan, G., Wang, L., Werner, C., and Butterbach-Bahl, K.: Potential benefits of liming to acid soils on climate change mitigation and food security, *Global Change Biology*, 27, 2807–2821, <https://doi.org/10.1111/gcb.15607>, 2021.
- Xu, T., Yuan, Z., Vicca, S., Goll, D. S., Li, G., Lin, L., Chen, H., Bi, B., Chen, Q., Li, C., Wang, X., Wang, C., Hao, Z., Fang, Y., and Beerling, D. J.: Enhanced silicate weathering accelerates forest carbon sequestration by stimulating the soil mineral carbon pump, *Global Change Biology*, 30, e17464, <https://doi.org/10.1111/gcb.17464>, 2024.
- 805 Xu, T., Li, H., Vicca, S., Goll, D. S., Beerling, D. J., Chen, Q., Bi, B., Yang, Z., Wang, X., and Yuan, Z.: Enhanced Rock Weathering Promotes Soil Organic Carbon Accumulation: A Global Meta-Analysis Based on Experimental Evidence, *Global Change Biology*, 31, e70483, <https://doi.org/10.1111/gcb.70483>, 2025.
- Yu, W.: Where and why do particulate organic matter (POM) and mineral-associated organic matter (MAOM) differ among diverse soils?, *Soil Biology and Biochemistry*, 2022.
- 810 Zhang, H.-M., Liang, Z., Li, Y., Chen, Z.-X., Zhang, J.-B., Cai, Z.-C., Elsgaard, L., Cheng, Y., Jan Van Groenigen, K., and Abalos, D.: Liming modifies greenhouse gas fluxes from soils: A meta-analysis of biological drivers, *Agriculture, Ecosystems & Environment*, 340, 108182, <https://doi.org/10.1016/j.agee.2022.108182>, 2022.
- Zhang, S., Reinhard, C. T., Liu, S., Kanzaki, Y., and Planavsky, N. J.: A framework for modeling carbon loss from rivers following terrestrial enhanced weathering, *Environ. Res. Lett.*, 20, 024014, <https://doi.org/10.1088/1748-9326/ada398>, 2025.